Materials Research. 2021; 24(suppl. 1): e20210013
DOI: https://doi.org/10.1590/1980-5373-MR-2021-0013

Low-cost supercapacitor based on colloidal graphite

***Maykel dos Santos Klem*[a]*, *Gabriel Leonardo Nogueira*[a], *Neri Alves*[a]**

[a]*Universidade Estadual Paulista (UNESP), Faculdade de Tecnologia e Ciências, 19060-900, Presidente Prudente, SP, Brasil.*

Received: January 08, 2021; Revised: July 17, 2021; Accepted: August 01, 2021

Here we report the production and characterization of a low-cost supercapacitor with electrodes based on colloidal graphite. We characterized the as-prepared device in terms of cyclic voltammetry (CV), Galvanostatic charge/discharge (GCD), and impedance spectroscopy. The supercapacitor exhibited good electrochemical performance with a high capacitance of 22 F g^{-1} for a discharge current of 2 mA. Long-term cyclability tests show that the device can keep about 85% of its capacitance after 500 cycles, even without encapsulation. We found power and energy densities of 110 W kg^{-1} and 3 Wh kg^{-1}, respectively. All the experimental results indicate that the colloidal graphite Aquadag® is a promising material for application in supercapacitors.

Keywords: *Colloidal Graphite; Aquadag; Supercapacitor; Energy Storage.*

1. Introduction

Energy storage devices, particularly supercapacitors, have attracted considerable attention in recent years because of the growing demand for electronic devices and gadgets[1,2]. Supercapacitors are energy storage devices that fill the gap between batteries and capacitors, providing high power with a reasonably high energy density[3]. They have been used in conjunction with batteries in electric vehicles and in hybrid electric vehicles to provide the necessary power during the car's ignition[4,5]. Recently, supercapacitors are also found in commercially available low-power electronics, *e.g.*, mobile, and wearable electronic devices[1,2]. In this context, the search for electrode materials that combine high performance, low-cost, and large-scale production is a current research trend.

In the past years, various materials have been studied as supercapacitor electrodes including carbon allotropes[6], metal oxides[7], conducting polymers[8], porous metal-organic frameworks (MOFs)[9-11], transition metal hydroxides (TMHs)[12], and their composites[13-15]. Particularly, carbonaceous materials have attracted much attention due to characteristics such as high specific area, high conductivity, good chemical stability, and relatively low-price[16-18]. Among the various carbon-based materials, graphene and carbon nanotubes stand out as promising materials for high-performance electrodes for supercapacitors[16,19]. These nanostructured materials provide electrodes with high surface area, high conductivity, and long-term cycle stability[20,21]. Furthermore, they allowed the fabrication of flexible carbon-based supercapacitors due to their mechanical properties[19,20]. Despite the many advantages, the high price compared to other carbonaceous materials and the small-scale production limit their application in commercially available supercapacitors.

Graphite is a low-cost carbonaceous material generally applied as a lubricant. Due to its high conductivity and the low specific area, the application of graphite in supercapacitors is restricted to the current collectors[22,23]. A specific type of artificial graphite was invented by E. G. Acheson in 1906, consisting of a colloidal dispersion. This material, commercially known as Aquadag®, was widely used in the past as a conductive coating in cathode ray tubes[24]. It is a low-cost material, when compared with other carbon-based materials, has high conductivity, and is produced on a large-scale[25]. Recently Aquadag® was mentioned in a work done by Sankar *et al.*, where it was utilized to produce graphene nanoplatelets to be applied in vanadium battery electrodes[26]. Another study has applied this material also in batteries as an anode electrode[27]. The use of the colloidal graphite Aquadag® in energy storage devices is restricted to batteries, and its application as supercapacitor electrodes has not been mentioned yet.

In this paper, we report the production of a low-cost supercapacitor using the commercial colloidal graphite as electrode material. We use a gel-like electrolyte composed of poly (vinyl alcohol) (PVA) and phosphoric acid (H_3PO_4), which works like an ionic conductor and dielectric separator. The as-constructed device presents a good electrochemical performance over cyclic voltammetry (CV), galvanostatic charge/discharge, long-term cyclability, and impedance spectroscopy (IS) measurements. Thus, we showed that Aquadag® is a suitable material for application in supercapacitors, with the advantage of being produced on a large scale.

2. Experimental

2.1. Electrolyte preparation

We prepared the gel-like electrolyte by adding 5 ml of phosphoric acid (1M – Sigma-Aldrich) into 40 ml of ultrapure water. This solution was heated until 90ºC and then added to it 5 g of Poly (vinyl alcohol) (PVA – Sigma-

*e-mail: *maykel.klem@unesp.br*

Aldrich). The solution was stirred at 85°C until complete solubilization of PVA.

2.2. Supercapacitor's assembly and characterizations

Two rectangular current collectors made of stainless steel (7,5 cm^2 each) were hand-coated in one side by colloidal graphite Aquadag® (Henkel) and left to dry for 5 minutes in room conditions. Then, the gel-like electrolyte was spread over Aquadag® electrodes and left to dry for 10 hours. After drying, the electrodes were pressed face-to-face to assemble the supercapacitor.

The morphology of the hand-coated film of Aquadag® was examined via scanning electron microscopy (SEM) (Carl Zeiss EVO LS15) images, with a working voltage of 30 kV. The vibrational characteristics of the material were analyzed using Raman Scattering Spectroscopy (Renishaw model in-Via) applying an excitation laser of 633 nm. The supercapacitor performance was studied through cyclic voltammetry and charge/discharge measurements, taken in a Keithley electrometer model 2420. Impedance spectroscopy was performed using an impedance analyzer from Solartron model 1260 with dielectric interface model 1296. All characterizations regarding the supercapacitor were performed using a two-electrode set-up.

3. Results and Discussion

Figure 1 shows SEM images in different magnifications for the manually deposited film of Aquadag®. The film presented an irregular surface mainly due to the deposition method. These surface irregularities enhance the specific surface area of the electrodes, consequently contributing to the improvement of the capacitance produced by the final device. We can see in Figure 1a that the film also presented some cracks, which were formed during the drying process. Although, this kind of failure will not affect the performance of the supercapacitor since the gel-like electrolyte will cover any defect in the film. It is shown in Figure 1b that the film is composed of micro flakes, which are probably comprised of the graphite present in the colloidal dispersion. These micrometric sized graphite flakes can also contribute to the capacitance of the device by allowing a high area in contact with the electrolyte.

We perform Raman spectroscopy measurements on the colloidal graphite to verify its vibrational characteristics. As we can see in Figure 2, the obtained Raman spectra exhibit the two characteristic peaks D and G for carbonaceous material, located at 1319 cm^{-1} and 1578 cm^{-1}, respectively[28]. The D peak is related to the defects and disorder degree of the material and arises from the symmetrical A_{1g} vibrational mode in carbon systems with sp^2 bonds. This vibrational mode only becomes active in the presence of disorder and does not appear for an ideal graphite crystal. The G peak occurs due to the in-plane stretching movement of carbon atoms and has E_{2g} symmetry[29]. The intensity ratio between the G and D bands I(D)/I(G) provides the structural order degree of the material. For the colloidal graphite, the I(D)/I(G) ratio was 1.15, a close value to those for highly disoriented materials as Pyrolytic carbon and glassy carbon[28]. In this way, the Raman spectroscopy shows that Aquadag® is formed mainly by disordered graphite. We performed a deconvolution on the Raman spectrum using the gaussian function due to the apparent presence of other peaks. As we can see in Figure 2, the deconvolution revealed three other peaks, I, D' and D". These peaks carry information about the ratio of sp^2 and sp^3 bonds (I), vacancy defects in the crystalline structure (D'), and the amount of amorphous carbon (D'')[30].

We performed impedance spectroscopy (IS) analyses on the supercapacitor at a frequency range of 0.01 Hz to 30 kHz. Figure 3 shows the obtained impedance spectrum for the IS analyses. The profile of the spectrum consists of a straight line with high inclination at low frequencies, and a semi-circle at high frequencies, as expected for supercapacitors[3]. To provide a better understanding of the IS characterization, we performed a curve fitting using equivalent circuits. The obtained circuit is shown in the inset of Figure 3. The values obtained by the curve fitting provided a good match to the experimental data, with a chi-squared of 10^{-4} [31]. All circuit parameters are summarized in Table 1.

The equivalent circuit shown in Figure 3 is composed of series resistance (R1) and a series inductance (L1), both in series with two parallel branches. The equivalent series inductance (L1) is a parasitic effect that can be related to the measurement system[32]. The series resistance (R1) is mainly related to the ionic resistivity of the electrolyte[33]. This parameter can be identified as the point where the spectrum touches the Z' axis in the high frequencies[34]. The second branch of the circuit is comprised of a CPE (CPE 1), in parallel with a resistance R2 in series with another CPE (CPE 2). This arrangement has the same structure as Randle's circuit, which is related to the interfacial phenomena of electrochemical

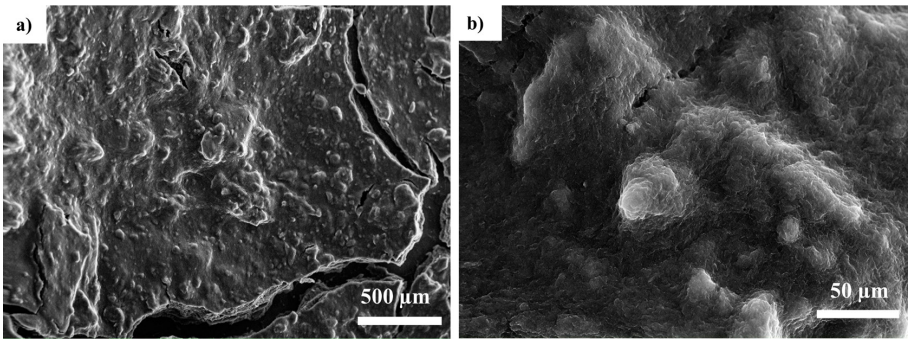

Figure 1. a), b) SEM images with different magnifications for the hand-coated film of Aquadag®.

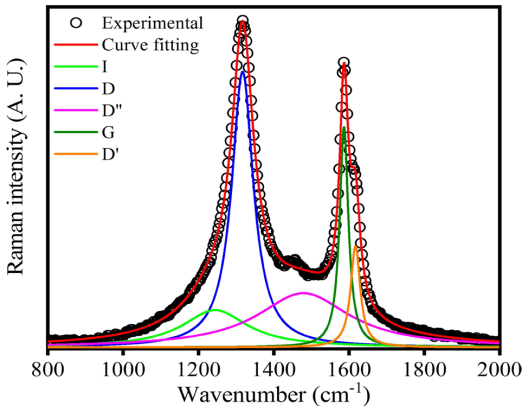

Figure 2. Raman spectra for the Aquadag® electrode. The hollow circles denote the experimental data; the red line is the total fit, and the other colored lines are the deconvoluted peak profiles.

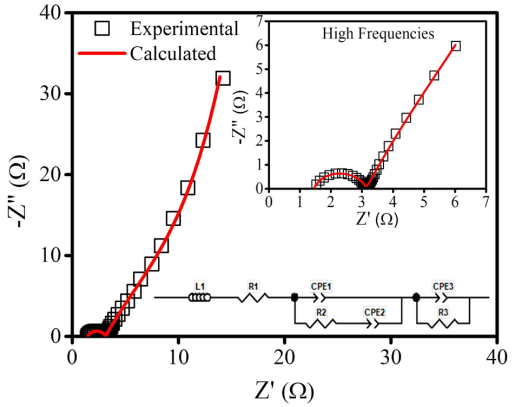

Figure 3. Nyquist plot for impedance data (hollow squares) and calculated values (line) obtained from the equivalent circuit for the supercapacitor. The inset shows the impedance spectra at high frequencies and the equivalent circuit model.

Table 1. Parameter values obtained from curve fitting.

Parameter	Values
L_1 (10^{-6} H)	2.4
R_1 (Ω)	1.2
Q_1 (10^{-4} Ω^{-1} s^n)	1.5
n_1	0.8
R_2 (Ω)	1.9
Q_2 (Ω^{-1} s^n)	5.0
n_2	0.9
R_3 (Ω)	11.9
Q_3 (Ω^{-1} s^n)	0.3
n_3	0.7

systems[35]. The parameter CPE is treated as time-constant distributions and may arise due to inhomogeneities on the film surface, differences in the film thickness, or other processes related to ion diffusion. The parameters CPE1 and CPE2 found on the equivalent circuit have been attributed to the non-ideal surface capacitance and the ion diffusion into the electrode, respectively[36].

The impedance of a CPE element can be described by $Z = 1/(Q(j\omega)^n)$. When n = 0, the CPE will behave like a resistance. For n=1, the CPE will be considered as a pure capacitance. When n=0.5, the CPE will produce the same impedance as a Warburg element, implying diffusion processes[37]. As seen in Table 1, the value n1=0.8, suggests a behavior closer to an ideal capacitance for the interfacial phenomena. The minor difference from the ideality (n=1) can be associated with the inhomogeneities of the electrodes, which generate a time-constant distribution. Furthermore, we found that n2=0.9 for the CPE2, showing that the kinetics of the electrode is not limited by ion diffusion. The R2 parameter represents the charge transfer resistance at the electrode/electrolyte interface[38]. This parameter can be identified in the impedance spectrum as the diameter of the semi-circle found in the high frequencies. The found value of 1.9 Ω suggests the good accessibility of charges to the electrodes. The parallel RC circuit represented by R3 and CPE3 fits the curve at the high frequencies. As can be seen in Table 1, n3=0.7, which suggests that the electrodes present mixed behavior between capacitance and diffusion mechanisms at low frequencies.

Figure 4a shows CV curves with scan rates varying from 1 to 50 mV s^{-1}. The curve profile shows a quasi-rectangular shape and is symmetric, indicating good capacitive behavior[39]. No redox peak was observed, as expected for carbon-based electrodes with electric double-layer storage mechanisms. The area contained by the voltammograms is proportional to the stored charge, and the device's capacitance (C) can be calculated from CV curves using[40]:

$$C = \int \frac{I(V)dV}{2n\Delta V} \quad (1)$$

where n represents the scan rate, ΔV the potential window, and $\int I(V)dV$ is the integral of one entire voltammetry cycle. Furthermore, in a two-electrode set-up the specific capacitance can be obtained as follows[41]:

$$C_{SP} = 2C/m \quad (2)$$

where C is the capacitance calculated from the CV curves, and m is the mass (g) of one electrode. Figure 4b shows the specific capacitances obtained for different scan rates. As can be seen, the specific capacitances tend to decrease as the scan rates rise. At low scan rates, the ions have more time to reach the inner and outer surfaces of the electrode, leading to a high measured capacitance. On the contrary, at high scan rates, only a small number of ions can reach the inner surfaces, producing a low capacitance[42]. In this way, the capacitance measured at low scan rates will give a better insight into the total capacitance produced by the electrode[43]. As shown in Figure 4b, we obtained a high specific capacitance of 20.2 F g^{-1} for a scan rate of 1 mV s^{-1}. Even for the high scan rate of 50 mV s^{-1}, the specific capacitance maintains a value of 6.5 F g^{-1}. In recent work, Ciszewski *et al.*reported a symmetric

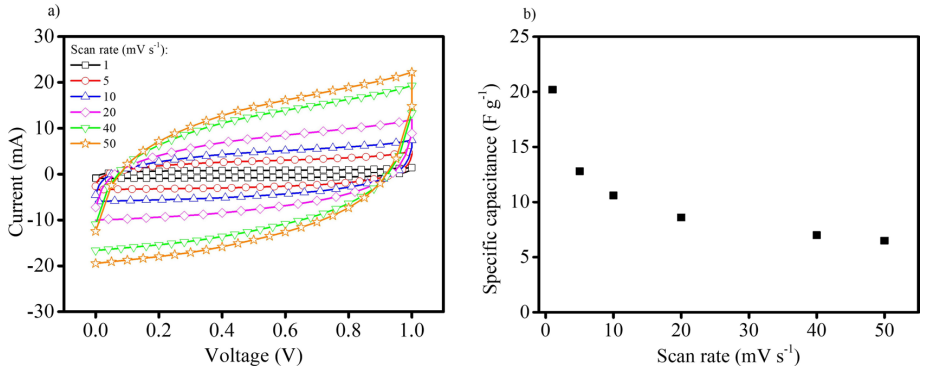

Figure 4. a) CV curves for supercapacitors with colloidal graphite-based electrodes at scan rates ranging from 1 to 50 mV s^{-1}. b) Specific capacitances calculated for various scan rates. The measurements were taken in a two-electrode set-up.

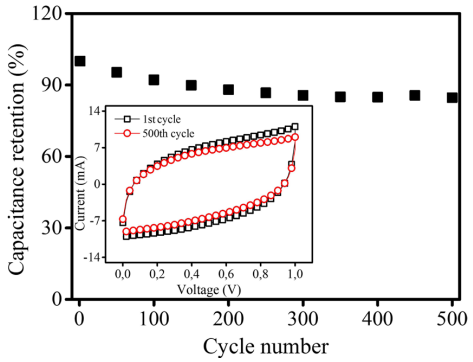

Figure 5. Capacitance retention vs. cycle number obtained from CV curves using a scan rate of 20 mV s^{-1}. The inset shows the CV curves for the 1st and 500th cycle.

supercapacitor with graphite-based electrodes with a low specific capacitance of 1.2 F g^{-1}[44]. In this same work, it is possible to see that our supercapacitor based on Aquadag® performed comparatively better than other carbon-based electrodes like multiwalled carbon nanotubes, carbon aerogels, and fullerene.

We performed long-term cycle stability tests along 500 CV cycle measurements using a scan rate of 20 mV s^{-1}, and the capacitance retention (%) vs. the number of cycles is depicted in Figure 5. We obtained that the capacitance is retained 85% of its initial value after 500 CV cycles. The inset of Figure 5 shows the CV curves for the 1st and 500th cycle. It is possible to notice that the shape of the 500th cycle curve is almost the same as the 1st cycle, presenting only a small reduction in the total area of the curve. The major decrease in capacitance retention is probably related to the drying of the electrolyte because the device was not encapsulated. Our device presented better cycle stability than other graphite-based supercapacitors found in the literature[44]. Usually, carbon-based supercapacitors have great cycle stability when compared to those based on electroactive materials[45].

We performed galvanostatic charge/discharge (GCD) analyzes applying current ranging from 2 to 10 mA, as can be seen in Figure 6a. The obtained curves showed a symmetrical triangular profile, demonstrating the good electrochemical capacitive behavior of the device. The capacitance was extracted from the discharge curves using[41]:

$$C = \frac{I}{\Delta V / \Delta t} \quad (3)$$

where ΔV is the potential variation at discharge and Δt the discharge time. Figure 6b shows the specific capacitance at different charge/charge currents obtained the specific capacitances by using Equation 2. We obtained a maximum specific capacitance of 22 F g^{-1} using a current of 2 mA as can be seen in Figure 6b. This value is higher than for a reported supercapacitor with reduced graphite electrodes[46]. Goucmuchi *et al.* reported a supercapacitor with nano-structural graphite electrodes with a specific capacitance of 12 F g^{-1}[47]. As seen in Figure 6b, the maximum specific capacitance drops by half when a charge/discharge current of 10 mA is used. Although, the device still can retain a great capacitance for a high current. The capacitance drop may be related to the charge/discharge kinetics. If the measurement is too fast, only a small number of charges will participate in the charge/discharge process, as seen for high scan rates in the CV analysis.

The energy (E) and power (P) densities are important parameters to evaluate the performance of a supercapacitor. E and P can be obtained from the specific GCD curves as follows[47]:

$$E = \frac{V^2}{7.2} x C_{SP} \quad (4)$$

$$P = 3600 x \frac{E}{t} \quad (5)$$

were V being the charge voltage, C_{sp} is the specific capacitance and t is the discharge time. Equations 4 and 5 allow to calculate the energy and power densities in Wh kg^{-1} and W kg^{-1}, respectively. Figure 7 presents the Ragone plot for the supercapacitor with electrodes based on Aquadag®. The maximum power and energy densities obtained were 110 W kg^{-1} and 3 Wh kg^{-1}, respectively. These values are comparable to other studies reporting carbon-based

Table 2. Comparison between Aquadag® and other carbon-based supercapacitors.

Electrode	Electrolyte	Specific capacitance (F g^{-1})	Energy density (Wh kg^{-1})	Power density (kW kg^{-1})	Capacitance retention (%)	Ref.
Graphite	6 M KOH	1.2	-	-	66.7% after 1000 cycles	[44]
Reduced graphite oxide	$BMIMBF_4$	6 at 1 A g^{-1}	-	-	-	[46]
Graphene-oxide/ activated carbon	PVA/H_3PO_4	20.8 at 5 A g^{-1}	2.9	0.05	-	[49]
Nano-structured Graphite	1 M Et_4NBF_4 + PC	12 at 1 mA	-	-	-	[50]
MWCNT sheet	1.96 M $TEMABF_4$ + PC	15	2.2	125	-	[51]
MWCNT/ PEDOT:PSS	PVA/H_3PO_4	20.3 at 1 mA	3.1	0.42	72% after 1000 cycles	[52]
Aquadag®	PVA/H_3PO_4	22 at 2 mA	3	0.11	85% after 500 cycles	This work

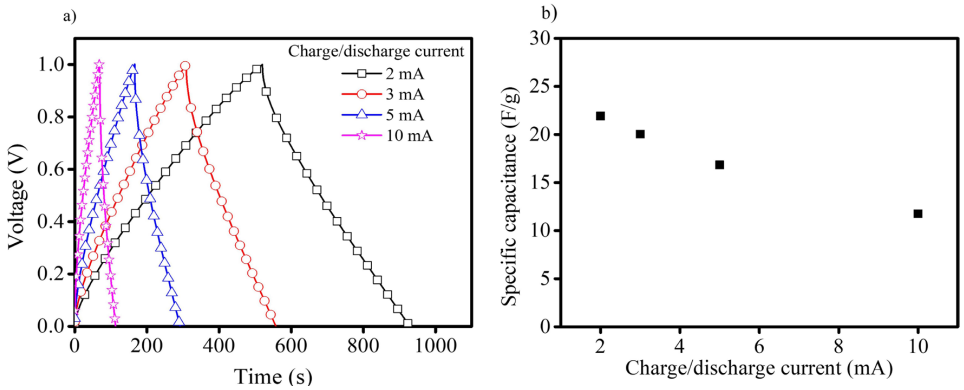

Figure 6. a) Charge/discharge curves with applied constant currents ranging from 1 to 10 mA for the supercapacitor using a two electrode set-up. b) Specific capacitance vs. the applied current. All the measurements were taken in a two-electrode set-up.

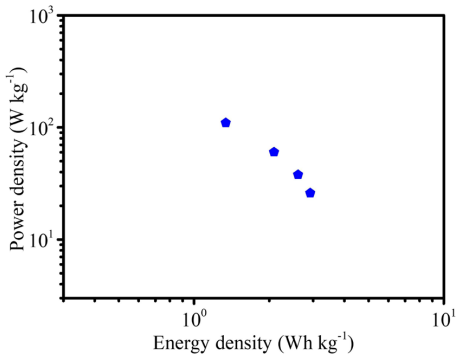

Figure 7. Ragone plots for the graphite-based supercapacitor with Power and energy densities calculated from the galvanostatic discharge curves.

supercapacitors[48]. Table 2 shows a comparison between our Aquadag®-based supercapacitor and other reported supercapacitors based on similar carbonaceous materials. Finally, the performance of the device demonstrated here makes Aquadag® a promising material for applications as supercapacitor electrodes.

4. Conclusions

In conclusion, we have successfully demonstrated for the first time the use of colloidal graphite Aquadag® as a low-cost supercapacitor electrode. The Raman spectroscopy characterization revealed that Aquadag® is composed of disordered graphite. The supercapacitor exhibited good electrochemical behavior in CV measurements, even at a high scan rate of 50 mV s^{-1}. We found a specific capacitance of 20.2 F g^{-1} for a scan rate of 1 mV s^{-1}. CDG curves also exhibited the good electrochemical behavior of the device, with a high specific capacitance of 22 F g^{-1} for a discharge current of 2 mA. We found power and energy densities of 110 W kg^{-1} and 3 Wh kg^{-1}, respectively. The device's capacitance is retained about 85% after 500 CV cycles, even without encapsulation. Finally, the performance obtained here makes Aquadag® a promising material for applications in low-cost supercapacitors.

5. Acknowledgments

Grant #2015/18091-8, São Paulo Research Foundation (FAPESP), Programa de Pós-graduação em Ciência e

Tecnologia de Materiais (POSMAT) and Instituto Nacional de Electrônica orgânica (INEO). This study was financed in part by the Coordenação de Aperfeiçoamento de Pessoal de Nível Superior - Brasil (CAPES) - Finance Code 001.

6. References

1. Raza W, Ali F, Raza N, Luo Y, Kim K-H, Yang J, et al. Recent advancements in supercapacitor technology. Nano Energy. 2018;52:441-73.
2. Cherusseri J, Choudhary N, Kumar KS, Jung Y, Thomas J. Recent trends in transition metal dichalcogenide based supercapacitor electrodes. Nanoscale Horizons. 2019;4:840-58.
3. Conway BE. Electrochemical capacitors: scientific fundamentals and technological applications. New York: Springer; 1999.
4. Zhang L, Wilkinson DP, Chen Z, Zhang J. Lithium-ion supercapacitors: fundamentals and energy applications. Boca Raton: CRC Press; 2018.
5. Hu S, Rajamani R, Yu X. Flexible solid-state paper based carbon nanotube supercapacitor. Appl Phys Lett. 2012;100:104103.
6. Frackowiak E, Béguin F. Carbon materials for the electrochemical storage of energy in capacitors. Carbon. 2001;39:937-50.
7. Lokhande CD, Dubal DP, Joo O-S. Metal oxide thin film based supercapacitors. Curr Appl Phys. 2011;11:255-70.
8. Mastragostino M, Arbizzani C, Soavi F. Conducting polymers as electrode materials in supercapacitors. Solid State Ion. 2002;148:493-8.
9. Liang Z, Zhao R, Qiu T, Zou R, Xu Q. Metal-organic framework-derived materials for electrochemical energy applications. EnergyChem. 2019;1:100001.
10. Wang K-B, Xun Q, Zhang Q. Recent progress in metal-organic frameworks as active materials for supercapacitors. EnergyChem. 2020;2:100025.
11. Li X, Yang X, Xue H, Pang H, Xu Q. Metal–organic frameworks as a platform for clean energy applications. EnergyChem. 2020;2:100027.
12. Duan H, Wang T, Wu X, Su Z, Zhuang J, Liu S, et al. CeO_2 quantum dots doped Ni-Co hydroxide nanosheets for ultrahigh energy density asymmetric supercapacitors. Chin Chem Lett. 2020;31:2330-2.
13. Frackowiak E, Khomenko V, Jurewicz K, Lota K, Béguin F. Supercapacitors based on conducting polymers/nanotubes composites. J Power Sources. 2006;153:413-8.
14. Li Y-Q, Shi H, Wang S-B, Zhou Y-T, Wen Z, Lang X-Y, et al. Dual-phase nanostructuring of layered metal oxides for high-performance aqueous rechargeable potassium ion microbatteries. Nat Commun. 2019;10:1-9.
15. Zheng S, Li Q, Xue H, Pang H, Xu Q. A highly alkaline-stable metal oxide@metal–organic framework composite for high-performance electrochemical energy storage. Natl Sci Rev. 2020;7:305-14.
16. Yang H, Kannappan S, Pandian AS, Jang J-H, Lee YS, Lu W. Graphene supercapacitor with both high power and energy density. Nanotechnology. 2017;28:445401.
17. Zhao D, Zhang Q, Chen W, Yi X, Liu S, Wang Q, et al. Highly flexible and conductive cellulose-mediated PEDOT:PSS/MWCNT composite films for supercapacitor electrodes. ACS Appl Mater Interfaces. 2017;9:13213-22.
18. Li J, Zhang W, Zhang X, Huo L, Liang J, Wu L, et al. Copolymer derived micro/meso-porous carbon nanofibers with vacancy-type defects for high-performance supercapacitors. J Mater Chem A Mater Energy Sustain. 2020;8:2463-71.
19. Xi S, Kang Y, Qu S, Han S. Flexible supercapacitors on chips with interdigital carbon nanotube fiber electrodes. Mater Lett. 2016;175:126-30.
20. Le LT, Ervin MH, Qiu H, Fuchs BE, Lee WY. Graphene supercapacitor electrodes fabricated by inkjet printing and thermal reduction of graphene oxide. Electrochem Commun. 2011;13:355-8.
21. Simon P, Gogotsi Y. Materials for electrochemical capacitors. Nat Mater. 2008;7:845-54.
22. Ramadoss A, Yoon K-Y, Kwak M-J, Kim S-I, Ryu S-T, Jang J-H. Fully flexible, lightweight, high performance all-solid-state supercapacitor based on 3-Dimensional-graphene/graphite-paper. J Power Sources. 2017;337:159-65.
23. Argüello JA, Cerpa A, Alanbari MH, Fariñas JC, Moreno R. Preparation of manganese oxide-graphite electrodes by electrophoretic deposition. Ceram Int. 2017;43:3231-7.
24. Szymanowitz R. Colloidal graphite. Its preparation, properties, and diversified uses in industry. J Chem Educ. 1939;16:413.
25. Venancio EC, Mattoso LHC, Júnior PS PH, MacDiarmid AG. Line patterning of graphite and the fabrication of cheap, inexpensive,"throw-away" sensors. Sens Actuators B Chem. 2008;130:723-9.
26. Sankar A, Michos I, Dutta I, Dong J, Angelopoulos AP. Enhanced vanadium redox flow battery performance using graphene nanoplatelets to decorate carbon electrodes. J Power Sources. 2018;387:91-100.
27. Tonti D, Pettenkofer C, Jaegermann W. In situ photoelectron spectroscopy study of a TiS_2 cathode in an operating battery system. Electrochem Solid-State Lett. 2000;3:220-3.
28. Chu PK, Li L. Characterization of amorphous and nanocrystalline carbon films. Mater Chem Phys. 2006;96:253-77.
29. Schreiber M, Lutz T, Keeley GP, Kumar S, Boese M, Krishnamurthy S, et al. Transparent ultrathin conducting carbon films. Appl Surf Sci. 2010;256:6186-90.
30. Kaplas T, Svirko Y. Direct deposition of semitransparent conducting pyrolytic carbon films. J Nanophotonics. 2012;6:061703.
31. Sarac AS, Sezgin S, Ates M, Turhan CM. Electrochemical impedance spectroscopy and morphological analyses of pyrrole, phenylpyrrole and methoxyphenylpyrrole on carbon fiber microelectrodes. Surf Coat Tech. 2008;202:3997-4005.
32. Ostafiychuk BK, Budzulyak IM, Rachiy BI, Kuzyshyn MM, Shyyko LO. Nanoporous nitrogencontaining coal for electrodes of supercapacitors. Nanoscience and Nanotechnology Research. 2013;1:17-22.
33. Lewandowski A, Olejniczak A, Galinski M, Stepniak I. Performance of carbon-carbon supercapacitors based on organic, aqueous and ionic liquid electrolytes. J Power Sources. 2010;195:5814-9.
34. Pandolfo AG, Hollenkamp AF. Carbon properties and their role in supercapacitors. J Power Sources. 2006;157:11-27.
35. Chen P, Chen H, Qiu J, Zhou C. Inkjet printing of single-walled carbon nanotube/RuO_2 nanowire supercapacitors on cloth fabrics and flexible substrates. Nano Res. 2010;3:594-603.
36. Sun W, Chen X. Preparation and characterization of polypyrrole films for three-dimensional micro supercapacitor. J Power Sources. 2009;193:924-9.
37. Taberna PL, Simon P, Fauvarque JF. Electrochemical characteristics and impedance spectroscopy studies of carbon-carbon supercapacitors. J Electrochem Soc. 2003;150:A292.
38. Mei BA, Munteshari O, Lau J, Dunn B, Pilon L. Physical interpretations of nyquist plots for EDLC electrodes and devices. J Phys Chem C. 2018;122:194-206.
39. Cheng Q, Tang J, Ma J, Zhang H, Shinya N, Qin LC. Graphene and nanostructured MnO_2 composite electrodes for supercapacitors. Carbon. 2011;49:2917-25.
40. Afraz A, Rafati AA, Najafi M. Optimization of modified carbon paste electrode with multiwalled carbon nanotube/ionic liquid/cauliflower-like gold nanostructures for simultaneous determination of ascorbic acid, dopamine and uric acid. Mater Sci Eng C. 2014;44:58-68.
41. Stoller MD, Ruoff RS. Best practice methods for determining an electrode material's performance for ultracapacitors. Energy Environ Sci. 2010;3:1294-301.
42. Pazhamalai P, Krishnamoorthy K, Manoharan S, Kim S-J. High energy symmetric supercapacitor based on mechanically

delaminated few-layered MoS_2 sheets in organic electrolyte. J Alloys Compd. 2019;771:803-9.
43. Dubal DP, Lee SH, Kim JG, Kim WB, Lokhande CD. Porous polypyrrole clusters prepared by electropolymerization for a high performance supercapacitor. J Mater Chem. 2012;22:3044-52.
44. Ciszewski M, Koszorek A, Radko T, Szatkowski P, Janas D. Review of the selected carbon-based materials for symmetric supercapacitor application. J Electron Mater. 2019;48:717-44.
45. Zhang LL, Zhao XS. Carbon-based materials as supercapacitor electrodes. Chem Soc Rev. 2009;38:2520-31.
46. Jha N, Ramesh P, Bekyarova E, Itkis ME, Haddon RC. High energy density supercapacitor based on a hybrid carbon nanotube–reduced graphite oxide architecture. Adv Energy Mater. 2012;2:438-44.
47. Kumar A, Kumar N, Sharma Y, Leu J, Tseng TY. Synthesis of free-standing flexible rGO/MWCNT films for symmetric supercapacitor application. Nanoscale Res Lett. 2019;14:1-17.
48. Zhang Y, Feng H, Wu X, Wang L, Zhang A, Xia T, et al. Progress of electrochemical capacitor electrode materials: a review. Int J Hydrogen Energy. 2009;34:4889-99.
49. Khawaja MK, Khanfar MF, Oghlenian T, Alnahar W. Fabrication and electrochemical characterization of graphene-oxide supercapacitor electrodes with activated carbon current collectors on graphite substrates. Comput Electr Eng. 2020;85:106678.
50. Gomibuchi E, Ichikawa T, Kimura K, Isobe S, Nabeta K, Fujii H. Electrode properties of a double layer capacitor of nano-structured graphite produced by ball milling under a hydrogen atmosphere. Carbon. 2006;44:983-8.
51. Honda Y, Haramoto T, Takeshige M, Shiozaki H, Kitamura T, Ishikawa M. Aligned MWCNT sheet electrodes prepared by transfer methodology providing high-power capacitor performance. Electrochem Solid-State Lett. 2007;10:A106.
52. Klem MS, Morais RM, Rubira RJG, Alves N. Paper-based supercapacitor with screen-printed poly (3, 4-ethylene dioxythiophene)-poly (styrene sulfonate)/multiwall carbon nanotube films actuating both as electrodes and current collectors. Thin Solid Films. 2019;669:96-102.